Regular Article

Heterogeneous Fenton-like surface properties of oxygenated graphitic carbon nitride

Wanessa L. Oliveira [a], Meiriele Antunes Ferreira [b], Henrique A.J.L. Mourão [b], Manoel J.M. Pires [b], Vinícius Ferreira [c], Honória F. Gorgulho [c], Daniel F. Cipriano [d], Jair C.C. Freitas [d], Valmor R. Mastelaro [e], Otaciro R. Nascimento [e], Dalva E.C. Ferreira [a], Frederico Ramos Fioravante [a], Márcio C. Pereira [f], João P. de Mesquita [a,*]

[a] Departamento de Química, Universidade Federal dos Vales Jequitinhonha e Mucuri, Rodovia MGT 367 - Km 583, n° 5000, Alto da Jacuba, CEP 39100-000, Diamantina, MG, Brazil
[b] Instituto de Ciência e Tecnologia, Universidade Federal dos Vales Jequitinhonha e Mucuri, Rodovia MGT 367 - Km 583, n° 5000, Alto da Jacuba, CEP 39100-000, Diamantina, MG, Brazil
[c] Departamento de Ciências Naturais, Universidade Federal de São João del Rei, Praça Dom Helvécio, 74, CEP 36301-160, São João del Rei, MG, Brazil
[d] Laboratory of Carbon and Ceramics Materials, Department of Physics, Federal University of Espírito Santo, Av. Fernando Ferrari, 514 - Goiabeiras, Vitória – ES, CEP 29075-910
[e] Instituto de Física de São Carlos, Universidade de São Paulo, Avenida Trabalhador São-carlense, 400, 13566-590, São Carlos, SP, Brazil
[f] Instituto de Ciência, Engenharia e Tecnologia, Universidade Federal dos Vales do Jequitinhonha e Mucuri, 39803-371, Teófilo Otoni, MG, Brazil

GRAPHICAL ABSTRACT
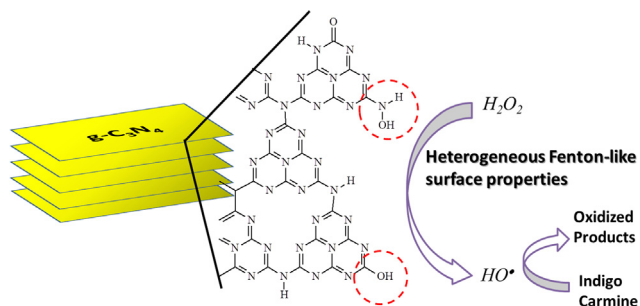
ARTICLE INFO

ABSTRACT

The photo-Fenton activity of graphitic carbon nitride (g-C_3N_4) has been widely studied, nevertheless, its Fenton-like catalytic behavior in the dark has not yet been demonstrated. In the present work, it is shown that oxygenated g-C_3N_4 obtained at different temperatures (500–600 °C) can degrade indigo carmine with hydrogen peroxide in the dark by a reaction similar to a conventional Fenton's reaction. Based on an extensive characterization of g-C_3N_4, we conclude that Fenton-like activity is directly related to the oxygenated functional groups on g-C_3N_4 structure, mainly by –OH functional groups. Oxygenated functional groups (e.g., hydroquinone-like groups) can reduce the H_2O_2 and generate oxidizing hydroxyl radicals, just like in the Fenton reaction performed by metals. In addition to new information on g-C_3N_4 surface reactivity revealed by this study, the metal-free oxygenated g-C_3N_4 catalyst may be an alternative to traditional metal catalysts used in Fenton-like reactions for advanced oxidation.

© 2020 Elsevier Inc. All rights reserved.

* Corresponding author.
  E-mail address: joao.mesquita@ufvjm.edu.br (J.P. de Mesquita).

1. Introduction

In the last century, metal-catalyzed chemical reactions have been widely used by the chemical industry to increase the efficiency and lower the costs of chemical processes [1]. Presently, the scientific community has sought to develop metal-free catalysts for use in traditional reactions developed over the past century and for recent demands such as advanced oxidation processes (AOPs) used to treat water contaminated with recalcitrant compounds [2–6]. However, due to typical Fenton reaction problems such as acidification and sludge formation, and the use of non-abundant elements [7,8], metal-free catalysts have been employed in the formation of oxidizing radicals in decontamination processes, especially using graphene-based materials catalysts [9–12]. Espinosa et al. showed that in the dark graphene can act as an effective heterogeneous Fenton-like catalyst [9].

Since research revealing graphitic carbon nitride (g-C_3N_4) as a photocatalyst for water splitting [13], first published in 2009, graphitic carbon nitride (g-C_3N_4) has become the new sensation in the field of photodevices due to its unique two-dimensional structure, the wide availability of their constituents, low cost, easy preparation, excellent thermal and chemical stability, and tunable electronic and optical properties [3,14,15].

The use of g-C_3N_4 in photo-Fenton reactions has been widely reported. However, g-C_3N_4 is usually associated with metal compounds [16–18]. Studies on metal-free g-C_3N_4 such as graphene@C_3N_4 2D heterojunctions and P- and S-doped g-C_3N_4 are less explored [19–24]. Cui et al. [21] prepared g-C_3N_4 from dicyandiamide at different temperatures and used the catalysts in the photo-Fenton reaction resulting in the degradation of organic dyes in aqueous solution. The authors performed an extensive study of the system, investigating the effect of pH and H_2O_2 concentration and the formation of oxygen radicals by ESR technique. In addition, they observed that the g-C_3N_4 remained unchanged after one cycle of rhodamine B (RhB) degradation. More recently, Tao et al. [25] investigated the peroxymonosulfate activation catalyzed by g-C_3N_4 under visible light. They also observed the formation of oxidizing sulfate radicals and the high stability of the g-C_3N_4 structure in multiple photocatalytic cycles.

Among the main strategies to improve the catalytic activity of graphitic carbon nitride are the preparation of nitrogen-deficient materials [26–29] and the functionalization with oxygenated functional groups [26,30–31]. In both strategies there is a change in the electronic structure of the materials, combined with the presence of oxygenated functional groups (NO, C=O, CO), alters the surface reactivity, and has provided a significant improvement in the catalytic activity of graphitic carbon nitride. Yu et al. prepared nitrogen-deficient g-C_3N_4 using a route based on hydrothermal polymerization in the presence of alkali [29]. The authors had noted the introduction of two types of nitrogen defects, vacancies and cyano functional groups. The presence of the defects promoted a redshift of the g-C_3N_4 absorption edge, which is proportional to the concentration of nitrogen defects. As a result, the authors observed a superior photocatalytic activity for the generation of hydrogen under visible light. Other authors have shown that the formation of defects in the g-C_3N_4 structure is associated with the formation of cyano and –OH functional groups [28]. On the other hand, Wei et al. have prepared oxygen-doped g-C_3N_4 via the solvothermal route and have shown that the presence of oxygenated functional groups increases electron donor density, electrical conductivity and mobility of charge carriers leading to an effective improvement in photocatalytic properties [30].

Although heterogeneous photocatalysis has great advantages over other catalytic processes, the difficulties in designing and scaling-up an efficient solar photoreactor with uniform distribution of sunlight inside of it can hinder its implementation. In this work we report on the ability of g-C_3N_4 to act as a Fenton-like heterogeneous catalyst in the dark at several pH values. The use of g-C_3N_4 in the development of a Fenton-like heterogeneous catalyst already has been reported, however, all studies use g-C_3N_4 in association with metallic compounds. Jiang et al. have prepared composites of g-C_3N_4 with nitrogen defects and copper oxides. They observed the formation of electron-rich centers capable of promoting the reduction of H_2O_2 to form HO• radicals, i.e., a Fenton-like reaction [28]. Bicalho et al. have prepared highly dispersed Fe(II)-doped g-C_3N_4 by simple calcination of an Fe^{3+}/melamine precursor. The authors verified a high Fenton-like catalytic activity for the degradation of different anionic, cationic and neutral compounds [31]. Here we show that the observed Fenton-Like catalytic activity is directly related to the unique structure of g-C_3N_4. Through a detailed investigation of the effect of the melamine heat-treatment temperature on the structure, surface chemistry, textural properties, and controlled oxidation of g-C_3N_4, we discuss the effect of oxygenated functional groups in the reduction of H_2O_2 to form highly reactive HO• radicals.

2. Experimental

2.1. Preparation of catalysts

Melamine (Sigma-Aldrich) was heat-treated for 2 h in a muffle furnace at different temperatures (300–600 °C) using a heating rate of 3 °C min^{-1}. Typically, 5 g of melamine were placed into an open ceramic crucible for the heat treatments. After 2 h, the samples were cooled naturally to room temperature. The g-C_3N_4 samples obtained at 500, 550 and 600 °C were named CNO-500, CNO-550 and CNO-600, respectively.

In order to evaluate the effect of a further oxidation on the catalytic activity, 50 mg of the sample C_3N_4-500 were added to 5 mL of H_2O_2 aqueous solutions (5 mol L^{-1}), and dispersed for 5 min in an ultrasonic bath (Digital Ultrasonic Cleaner, Model CD-4860). After dispersion, the solution was refluxed for 2 h at 80 °C. After cooling down to room temperature, the sample was centrifuged, washed with deionized water and ethanol and dried in an oven for 24 h at 100 °C.

2.2. Characterization

X-ray diffraction (XRD) data were obtained in a Shimadzu diffractometer model XRD6000 with a current of 30 mA, voltage of 30 kV, and Cu Kα radiation. FTIR spectra were obtained in a Varian 640ir spectrometer using the GladiATR™ accessory (Pike instruments). The potentiometric titration curves were recorded with a SCHOTT automatic titrator (Titroline 7000) using a combined pH electrode model HI-1110 (Hanna instruments) as described elsewhere [32–34]. The elemental composition (CHNS) was obtained with a LECO®CHNS/O analyzer, model TruSpec Micro. Solid-state NMR experiments were performed at room temperature in a Varian/Agilent VNMR 400 MHz spectrometer (magnetic field of 9.4 T, ^{13}C NMR frequency of 100.52 MHz), using a triple-resonance probehead; the powdered samples were packed into zirconia rotors (with 4 mm diameter) for magic angle spinning (MAS) experiments at the spinning rate of 14 kHz. The materials were analyzed using a ^{1}H–^{13}C cross-polarization (CP) pulse sequence, with a π/2 ^{1}H excitation pulse of 3.6 µs, a recycle delay of 5 s, a contact time of 10 ms (chosen after optimization), a spectral window of 250 kHz and 2200 accumulated transients; high-power ^{1}H

decoupling (SPINAL method) was employed during the recording of the free induction decays (FIDs), with an acquisition time of 16.38 ms. All ^{13}C NMR spectra were obtained by Fourier transform of the FIDs, after applying a line broadening of 50 Hz (CP spectra); the chemical shifts were referenced to tetramethylsilane (TMS), using hexamethylbenzene as a secondary reference (signal at 17.3 ppm).

X-ray photoelectron spectroscopy (XPS) was performed by using a ScientaOmicron ESCA+ spectrometer with a high-performance hemispheric analyzer (EA 125), using monochromatic Al Kα (1486.6 eV) radiation as the excitation source. The operating pressure in the ultra-high-vacuum (UHV) chamber during the analysis was 2×10^{-9} mbar. Pass energies of 50 and 20 eV were used for the wide range survey and high-resolution spectra, respectively. The following signals were used for the analysis: O 1s, C 1s and N 1s. The (CH)n component of the C 1s peak of adventitious carbon was fixed at 284.5 eV to set the binding energy scale. The chemical states were identified considering reported values of binding energies [35–38]. CasaXPS software was used for the data analysis with Shirley backgrounds and assuming the occurrence of Voigt-shaped peaks.

The specific areas of g-C$_3$N$_4$ samples were determined by N$_2$ adsorption, according to the BET method, using a Quantachrome Autosorb-2 instrument. All the data analyses were performed using ASiQWin v.1.11 software (Quantachrome).

2.3. Heterogeneous Fenton-like reaction and DMPO test

The Fenton-like catalytic activity of g-C$_3$N$_4$ samples was determined by monitoring the optical absorption band intensity of indigo carmine (IC) dye at 610 nm for various reaction times. In short, 15 mg of the different samples prepared by thermal polycondensation of melamine were placed in 30 mL of 20 mg L^{-1} IC solution. After the IC adsorption, 10 μL of H$_2$O$_2$ (35% wt) was added. The IC solutions were also adjusted with HCl and NaOH solutions to evaluate the effect of pH on the Fenton-like activity of g-C$_3$N$_4$ samples. The rate constants for the IC discoloration were estimated using the Langmuir-Hinshelwood kinetic model [39,40].

The hydroxyl radicals (HO$^\bullet$) generated by the g-C$_3$N$_4$ sample treated at 600 °C were determined by using DMPO as spin trap and electron paramagnetic resonance (EPR) spectroscopy at room temperature. The suspension was prepared by dispersing 1.0 mg of g-C$_3$N$_4$ (prepared at 600 °C) in 3.0 mL of 20 mg L^{-1} IC solution. After 10 min of magnetic stirring, the DMPO was added into 200 μL of this suspension to obtain a 30 mM DMPO solution. After that, 70 μL of H$_2$O$_2$ (35%) was added into this suspension, which was placed into an EPR cell. This main mixture test was identified as g-C$_3$N$_4$ + IC + DMPO + H$_2$O$_2$. The control samples (IC + DMPO, g-C$_3$N$_4$ + IC + DMPO and IC + DMPO + H$_2$O$_2$) were analyzed in a similar procedure. Furthermore, an additional measurement using the mixture g-C$_3$N$_4$ + IC + DMPO + H$_2$O$_2$ was done after 70 min inside EPR cell without either the magnetic stirring or lighting. The spectra were acquired at 25 °C in a Varian E109 X-band instrument with a standard rectangular cavity using a glass quartz flat cell (Wilmad). Measurement conditions were: center field of 3390 Gauss, sweep field of 160 Gauss, sweep time of 60 s, microwave (MW) power of 10 mW, gain of 2.0×10^3, modulation amplitude of 0.5 Gauss, modulation frequency of 100 kHz, time constant of 0.064 s and MW frequency of 9.517727 GHz. Spectral simulations were obtained using the EasySpin program [41] with the following EPR parameters for DMPO OH radical adduct: g = 2.0056, line width = 1.09 Gauss, AN = 15.14 Gauss, AH = 14.97 Gauss.

3. Results and discussion

XRD patterns show that the melamine structure begins to be changed from 350 °C and the formation of the graphitic structure starts at 450 °C. From 500 °C the typical diffraction pattern for g-C$_3$N$_4$ is observed, with the presence of the diffraction peaks centred at 2θ = 27.5° and 13.0°, which are characteristic of the (002) and (100) planes, respectively (Fig. 1) [42].

The FTIR technique was used to obtain complementary information about the g-C$_3$N$_4$ structure under different heating temperatures. The spectra obtained are shown in Fig. 2. The spectra of the melamine and the sample treated at 300 °C are very similar (Fig. 2a). The sharp band around 810 cm^{-1} is assigned to the breathing mode of triazine units, while the bands at 1570 and 1634 cm^{-1} are attributed to N—H bending and stretches of the C=N bonds. The bands between 1258 and 1480 cm^{-1} were attributed to stretches of C—N bonds [43]. The bands between 3000 and 3300 cm^{-1} are derived mainly from the stretches of the N—H bonds [44].

As in XRD patterns, the FTIR spectra show the beginning of the structural modification of melamine from 350 °C, which are similar to those obtained at 400 °C and 450 °C. In this range of temperatures progressive changes in the FTIR spectra were observed. On the other hand, a similar pattern is observed for the spectra of g-C$_3$N$_4$ samples obtained at temperatures above 500 °C. The changes in the absorptions are clearer in the spectra obtained from 500 °C, in the region of 3000–3300 cm^{-1}, relative to the precursor, which indicates the condensation of –NH$_2$ groups. In this region three bands between 3170 and 3300 cm^{-1} can be verified, mainly in the spectrum of the sample prepared at 600 °C, typical of N—H stretch of primary and secondary amines and, O—H stretching formed during thermal polycondensation of melamine. The oxygenated functional groups can be identified from a more detailed analysis in the 900–1800 cm^{-1} region (Fig. 2C). The centered shoulder at 1680 cm^{-1} in the g-C$_3$N$_4$ sample prepared at 600 °C is typical
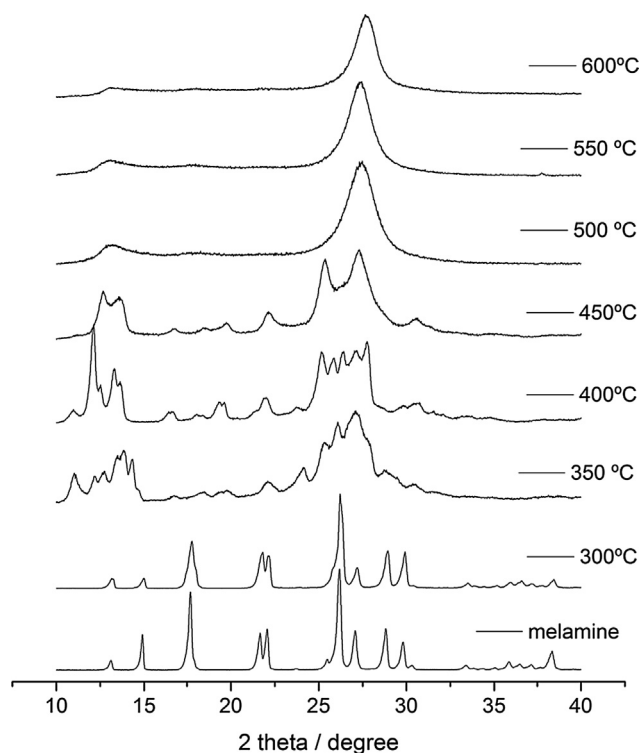

Fig. 1. XRD patterns obtained for melamine heat-treated at different temperatures.
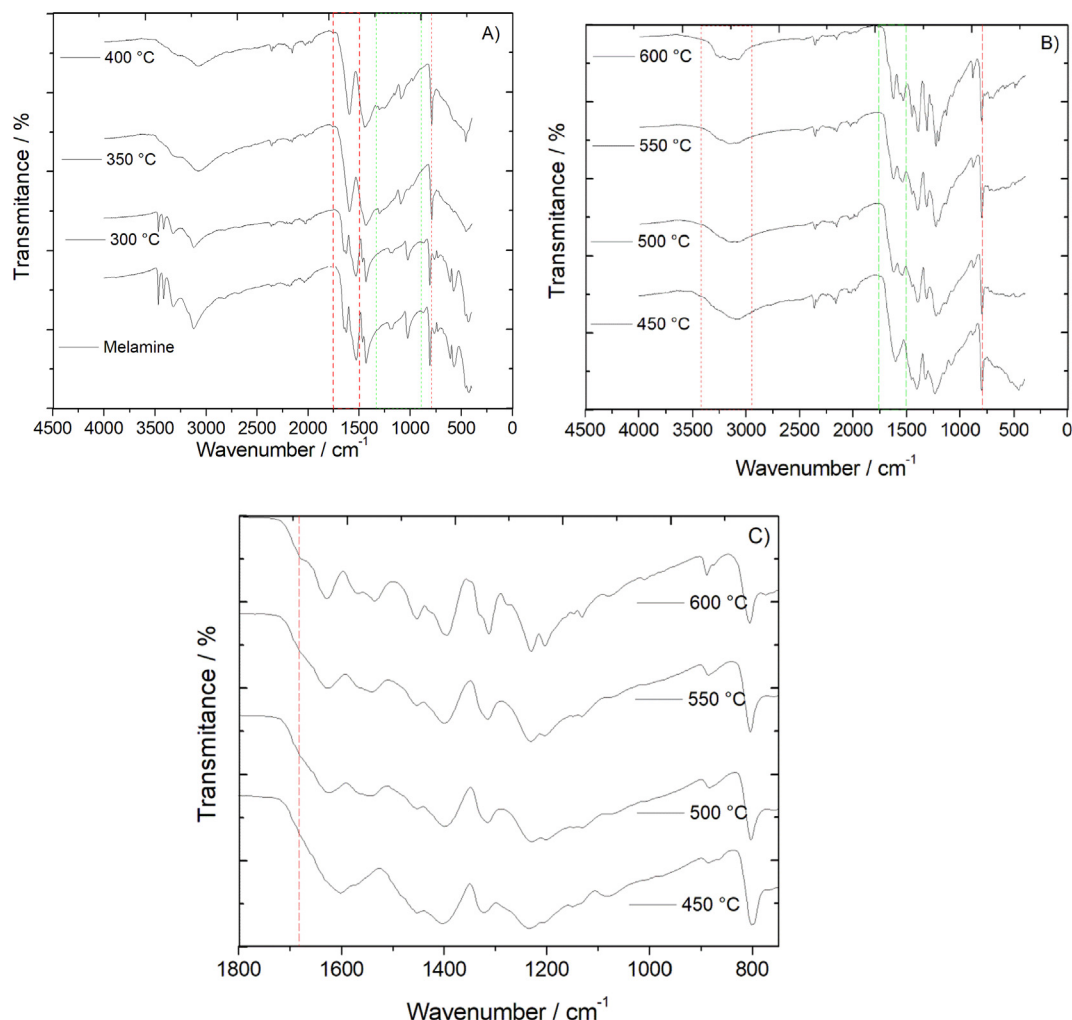
Fig. 2. FTIR spectra patterns obtained for melamine heat-treated at different temperatures (A, B). C) Amplification of the region between 1800 and 900 cm^{-1} of the spectra shown in B.

Table 1
Elemental composition (CHN-O analysis) obtained for oxidized g-C$_3$N$_4$ samples and melamine.

Samples	C (wt%)	N (wt%)	H (wt%)	O* (wt%)	C/N (atomic ratio)
Melamine	28.6	66.5	4.8	–	0.50
CNO-500	32.0	57.3	1.6	9.1	0.65
CNO-550	33.2	59.2	1.4	6.2	0.65
CNO-600	30.1	53.5	1.6	14.8	0.65

* Obtained by mass difference.

of carbonyl functional groups. These functional groups can modify the texture and electronic properties of g-C$_3$N$_4$ favoring its catalytic properties [45,46].

The oxygen in the g-C$_3$N$_4$ structures was quantitatively confirmed by elemental analysis (Table 1). The molecular formula of melamine is C$_3$N$_6$H$_6$ and the molecular formulas of g-C$_3$N$_4$ obtained at 500, 550, and 600 °C are C$_3$N$_{4.6}$H$_{1.8}$O$_{0.6}$, C$_3$N$_{4.6}$H$_{1.5}$O$_{0.4}$ and C$_3$N$_{4.6}$H$_{1.8}$O$_{1.1}$, respectively. The molar mass increases from 111.8 g mol^{-1} (500 °C) to 118.4 (600 °C) due to the oxygen in the graphitic structure.

Since many nitrogenous and oxygenated functional groups have Brønsted acidity, the acid-base properties of the materials were investigated. The obtained titration curves are shown in Figure S1 (supplementary data). The melamine titration curve shows a buffering region in the pH range of 4.5–5.5. The multiparameter

adjustment of the titration curve shows a pKa of 5.1, characteristic of the conjugate acid of melamine, with a concentration of 7.9 mmol g^{-1} (Table S1). The other two pKas can be attributed to impurities or even carbonates. The results obtained at 300 °C are similar to those of melamine, since at this temperature the melamine structure changes slightly. However, from 350 °C a significant decrease of the acid functional groups indicates the beginning of the condensation reaction of the structures. From 400 °C the total acid functional groups increase until the temperature of 600 °C due to increased oxidation of the g-C$_3$N$_4$ (Table S2). The acidity of g-C$_3$N$_4$ is directly related to the presence of primary, secondary, tertiary amines (–NR$_2$H$^+$ → –NR$_2$ + H$^+$) and optionally, oxygenated functional groups such as carboxylic and hydroxyl groups. The acidity of these nitrogenous and oxygenated groups provides an isoelectric point of less than 7, typically around 5 [47].

3.1. Fenton-like heterogeneous catalysis

In some photocatalytic tests with g-C$_3$N$_4$/metal oxide heterostructures, we observed that some samples have high catalytic activity using H$_2$O$_2$ in the dark (see supplementary information, Figure S2). Therefore, we investigated in more detail the heterogeneous Fenton-like activity of g-C$_3$N$_4$ samples for the IC degradation. The indigo carmine (IC) optical absorption spectra at different reaction times using g-C$_3$N$_4$ catalysts and H$_2$O$_2$ in the dark were obtained and the relative concentrations to the initial concentration (I/I$_0$) at different times are shown in Fig. 3. Figure S3 shows a comparison between adsorption and discoloration of the dye IC for the sample obtained at 600 °C.

The highest catalytic activities were observed for g-C$_3$N$_4$ samples calcined at 500–600 °C, showing that the structure of the graphitic carbon nitride plays an essential role on catalytic activity. The typical pseudo-first order kinetic model was used to fit the data (Fig. 4). The apparent rate constant (k′) obtained from the slope of these lines are shown in Table S3. The g-C$_3$N$_4$ sample obtained at 600 °C was the most efficient, almost completely degrading the dye in 50 min with a kinetic constant of 37.4×10^{-3} min^{-1}. Once the effectiveness of the g-C$_3$N$_4$ structure on catalytic activity had been demonstrated, we focused our attention on the surface and textural properties of the samples obtained at different calcination temperatures. The specific areas obtained by nitrogen adsorption isotherms were 11.1, 45.2 and 19.3 m^2 g^{-1} for samples prepared at 500, 550 and 600 °C, respectively. Typically, the surface areas reported for g-C$_3$N$_4$ are between 10 and 40 m^2 g^{-1} [15]. Here, g-C$_3$N$_4$ obtained at 550 °C showed the largest surface area of 45 m^2 g^{-1}.

Fig. 5 shows that catalytic activity has no clear relation to the surface area of the g-C$_3$N$_4$, since the sample with the larger surface area shows the smaller catalytic activity. On the other hand, analyzing the results of the elemental composition (Table 1) and those shown in Table S3, we observed an evident relationship between the catalytic activity and the oxygen concentration present in the structure of the g-C$_3$N$_4$ samples. To prove the positive impact of oxygenated functional groups on discoloration of the indigo carmine dye, we prepared a sample of g-C$_3$N$_4$ under nitrogen atmosphere at 600 °C. The g-C$_3$N$_4$ sample obtained under inert atmosphere actually has very slow kinetics compared to the sample obtained in the air atmosphere (Figure S4). In addition, we
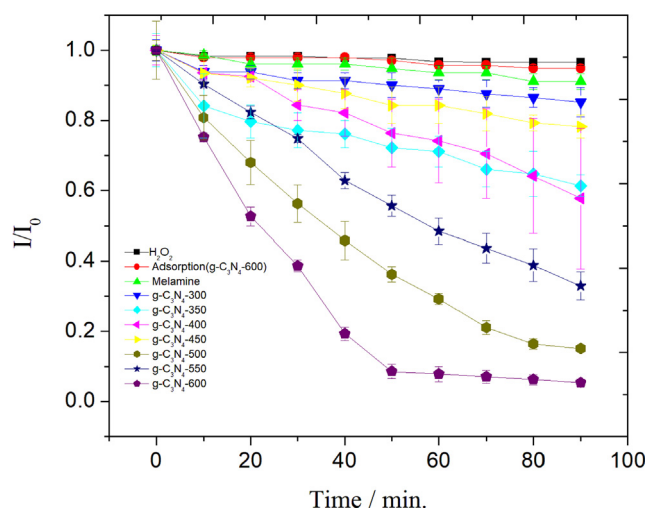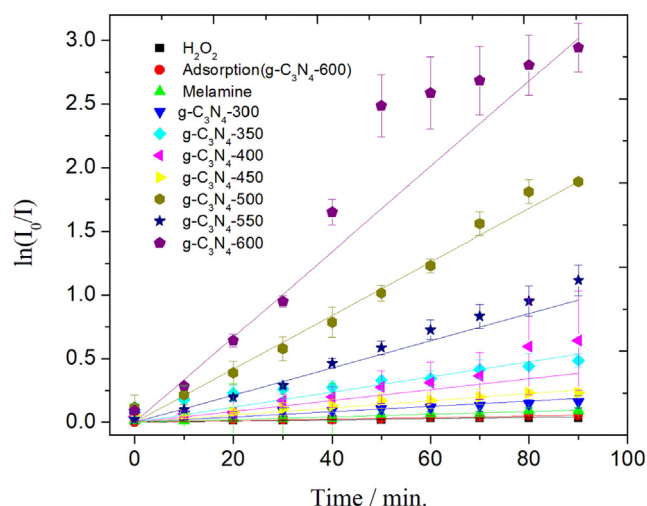

Fig. 4. Kinetic analysis (Langmuir-Hinshelwood kinetic model) of the IC kinetic discoloration using melamine treated at different temperatures and hydrogen peroxide. Note: The g-C$_3$N$_4$ samples were obtained at temperatures of 500, 550 and 600 °C.
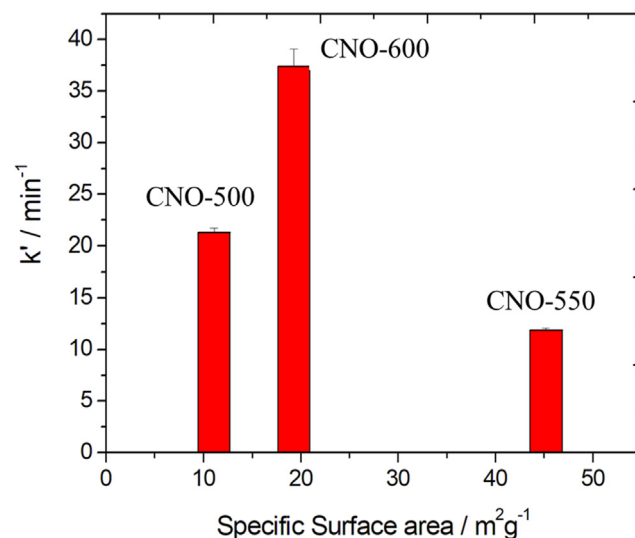

Fig. 5. Effect of the specific surface area on the pseudo-first order kinetic constant obtained for the discoloration of IC dye by heterogeneous Fenton-like catalysis.

noted that the Fenton-like activity increases linearly with the oxygen concentration on the g-C3N4 (Fig. 6).

Solid-state ^{13}C NMR and XPS experiments were also carried out in order to identify the oxygenated functional groups present in the g-C$_3$N$_4$ structure. The ^{13}C CP/MAS NMR spectra obtained for the g-C$_3$N$_4$ samples prepared at different temperatures are shown in Figure S5. The spectra show the typical signals at 157 and 165 ppm attributed to the groups CN3 (Ci) and CN2NH2 (Ce) (Figure S5a), respectively [48]. At first, the signals obtained for the samples prepared at different temperatures are very similar, but a more detailed analysis of these peaks (Figure S5b) reveals a singular asymmetry at the peak centered at 165 ppm for the sample obtained at 600 °C. This shoulder can be ascribed to the presence of oxygen functional groups (e.g., carbonyl groups) associated with the Ce carbon. In addition, the ratio between the Ci and Ce peak areas in the spectrum obtained for this sample (0.80) is lower compared to the samples prepared at 500 °C (0.87) and 550 °C (0.87). Although the spectra recorded with CP are not quantitative, this

Fig. 3. IC dye kinetic discoloration using melamine treated at different temperatures and hydrogen peroxide. Note: The g-C$_3$N$_4$ samples were obtained at temperatures of 500, 550 and 600 °C. Conditions: pH = 6, [IC] = 20 mg L^{-1} and [H$_2$O$_2$] = 3.9×10^{-3} mol L^{-1}.

W.L. Oliveira, Meiriele Antunes Ferreira, Henrique A.J.L. Mourão et al.

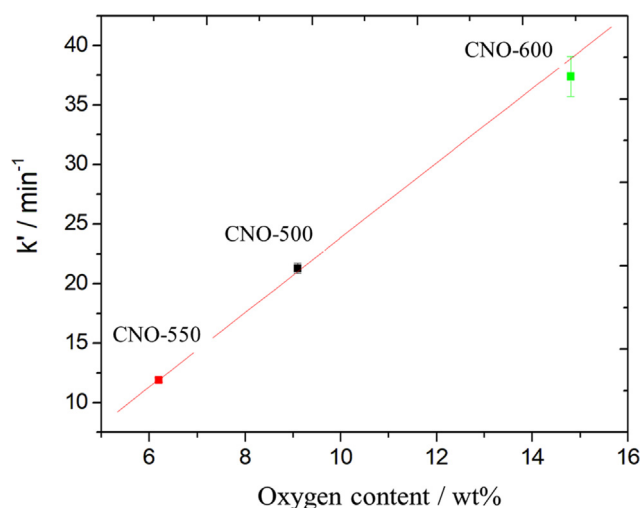*Journal of Colloid and Interface Science 587 (2021) 479–488*

Fig. 6. Effect of oxygen content on the pseudo-first order kinetic constant obtained for the discoloration of IC dye by heterogeneous Fenton-like catalysis.

comparison between relative intensities of spectra recorded under the same experimental conditions suggests an increase in the relative concentration of the Ce carbon atoms with the increase in the heat treatment temperature. This can be caused by the breakdown of the tertiary amine bonds that bind the heptazine fragments in the g-C_3N_4 structure or of the *s*-triazine rings with the insertion of oxygenated functional groups, for example, hydroxyl groups [28,49]. We have observed that at temperatures above 600 °C (i.e., 650 °C), the synthesis yield of g-C_3N_4 is practically zero due to decomposition of the material under this condition. The wide range XPS spectra and the fittings for each detected element are presented in the supplementary material (Figure S6). The atomic composition of the g-C_3N_4 surfaces calculated from the wide range XPS scans is presented in Figure S7. The overall amounts of carbon and oxygen increased, and the nitrogen content decreased as the temperature of treatment enhanced. Similar results have been observed by other authors [46,50]. Yang et al. observed a C/N ratio close to 1 for g-C_3N_4, thermally oxidized at 550 °C [50]. In comparison with the data presented in Table 1, it should be emphasized that XPS signals come from surface of the samples, and then different atomic percentages are expected between these techniques.

The high-resolution spectra for C1s, N1s, and O1s XPS are shown in Fig. 7 and the detailed parameters obtained from the fits are presented in Table S4. The spectra N1s of the three samples submitted to calcination are very similar each other but distinct from that of melamine, mainly in the range from 400 to 405 eV. In this range, the calcined samples have presented two additional signals. The more intense part of the N1s spectra, between 397 and 400 eV, was fitted with two signals centered at 398 and 399 eV, which correspond to N in the structures C=N-C and C-NH_2, occurring in both melamine and g-C_3N_4 [35–38,51]. The signal at 399 eV can also be attributed to N—C—OH structures [52].

The two additional signals centered at 400.5 and 403.8 eV, can be associated to N in the groups NC3 and N—O terminated, respectively [37,38,51]. This last signal may be related not only to pyridine-like N-oxide but also to N in a structure similar to N in heterocycles associated to the pair -N^+-O^- or even in the N-OH group. In order to simplify the text, the signals associated to these possibilities will be referred as "PNO". Regarding the signal centered at 400.5 eV, it also can be associated to quaternary-N [51], or to nitrogen in N-C=O structures, which also can be present but not unequivocally distinguished in these spectra [52]. Besides

those signals, an additional signal at about 405.8 eV was due to the π-excitations of N. The relative percentages of the contributions to the N 1s XPS spectra are presented in Fig. 8.

The relative amounts of N in binding energies of 398.0 and 399.0 eV are close to each order. In melamine the distribution of N in these of types of bonding, C=N-C and C-NH_2, is 1:1 [38,53]. In the sample treated at 600 °C, the amount of N in C=N-C is significantly smaller than the amount of N in functional groups with binding energy of 399 eV. Furthermore, the relative amount of N in C=N-C decreases from the melamine to the other samples as the treatment temperature increases, indicating that the thermal treatment favors the break of C=N double bonds. The reduction of this type of bonding is concomitant with the formation of NC_3 (400.5 eV) and PNO (403.8 eV), or even with the formation of O=C-N (400.5 eV).

Regarding the O 1s XPS spectra, the sample treated at 600 °C was the one presenting more differences. Besides the larger content of oxygen in this sample, the XPS results point to a smaller fraction of oxygen forming H_2O and a larger fraction forming –OH and PNO, as compared with the other samples. The spectra were fitted with these two signals, with oxygen from H_2O appearing at approximately 533.1 eV and from –OH and/or PNO at ~531.7 eV [37]. The overlap between the signals does not permit the precise quantification of each one of these compounds, and the occurrence of C=O and C—O cannot be disregarded. Some authors have shown that O atoms could be directly bonded to sp^2-hybridized carbon on oxidized g-C_3N_4 [54]. C1s peaks were fitted with two signals interpreted as (CH)n at 284.5 eV and C bonded to N at about 287.7 eV. This last signal is in fact the result of the overlap contributions of C in different groups as N2CH2, N = CN2 and NC3. The resolution is not enough to distinguish these contributions, but full width at half maximum between 1.8 and 2.1 eV can be seen as an indication of the overlap [36,53]. The presence of groups of C=O and C—O in small amounts cannot be disregarded since their binding energies for C 1s are in the same range [37]. The signal from C in the PNO also cannot be distinguished in the overlapped contributions to C 1s, but its presence has been evidenced by N 1s XPS spectra. Fig. 9 presents the relative percentages of the two C signals fitted to the XPS spectra. One can see the relative amount of C bonded to N decreases significantly only for the sample calcined at 600 °C.

Due to the difficulty of differentiating oxygenated and nitrogenous functional groups, the identification of the functional groups in the g-C_3N_4 structure, obtained at different temperatures, is challenging. The formation of oxidizing radicals through the reaction with amine groups, widely available throughout the graphitic carbon nitride structure, should be considered, since the radical reactions with these compounds are widely known and studied [55]. In fact, the nitrogen atoms present high electronic density, with the valence band of the formed g-C_3N_4, predominantly associated with their p_z orbitals [13]. Thus, amine groups on the g-C_3N_4 surface favor the formation of oxidizing radicals. However, theoretical studies show increased reactivity of N-doped graphene for the reduction of H_2O_2, but without radical formation [56]. On the other hand, we observe a greater amount of oxygenated functional groups in the sample obtained at 600 °C.

The H_2O_2 adsorption is an essential step for subsequent reactions of H_2O_2 with the functional groups present on the surface of g-C_3N_4 [56]. Thus, the Density Functional Theory (DFT) was applied with M06 functional and 6-31G(d,p) basis set for all atoms in order to investigate the adsorption energy using simplified models containing these oxygenated and nitrogenous functional groups. The results show a decrease in system energy indicating that the adsorption process is energetically favorable. It was also observed that the decreasing energy is less pronounced when the oxygen is absent of the structure model, showing the same trend
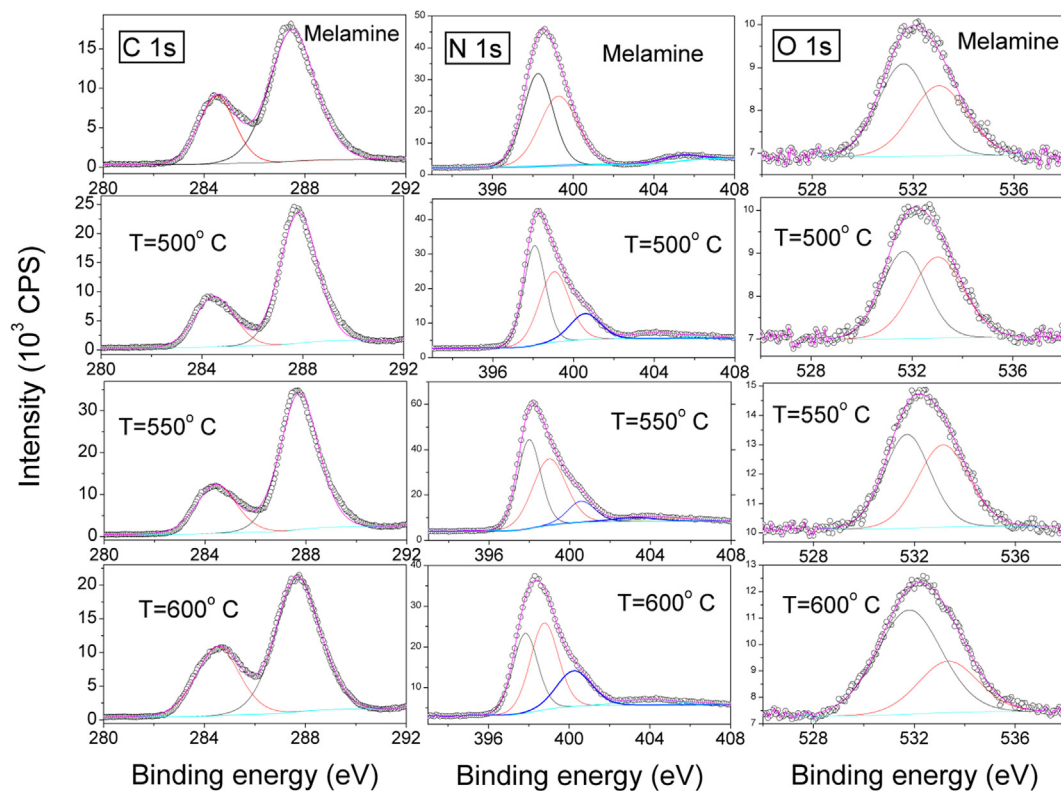
W.L. Oliveira, Meiriele Antunes Ferreira, Henrique A.J.L. Mourão et al.

Journal of Colloid and Interface Science 587 (2021) 479–488

Fig. 7. High resolution C1s, N1s, and O1s XPS spectra of g-C$_3$N$_4$ samples prepared at 500 (CNO-500), 550 (CNO-550) and 600 °C (CNO-600).
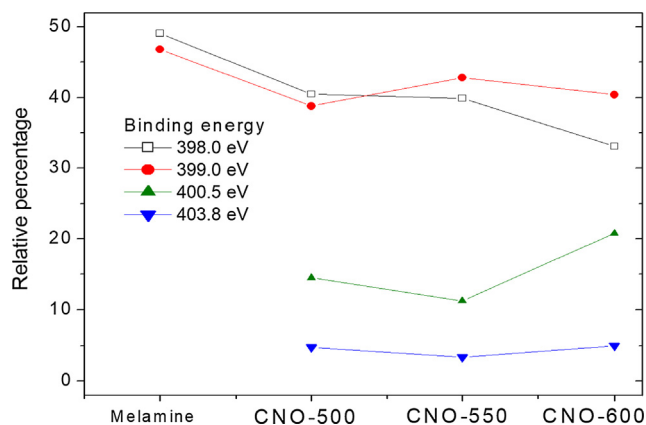

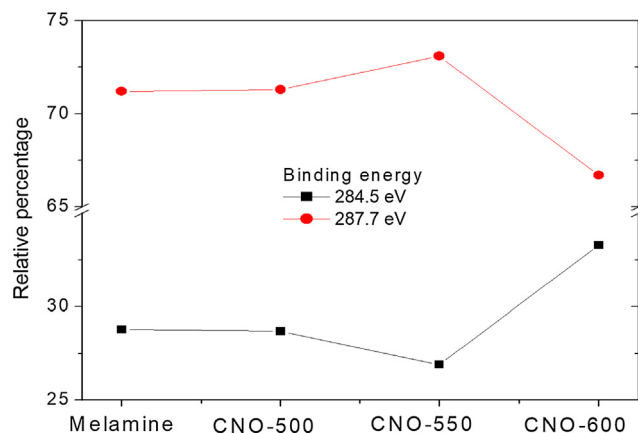**Fig. 8.** Relative percentages of the components used to fit the N1s XPS spectra.

Fig. 9. Relative percentages of the components used to fit the C1s XPS spectra.

that was observed in the experiment. This result is consistent with the assumption that the dye discoloration rate rises with the oxidation of the g-C$_3$N$_4$. The interaction between H$_2$O$_2$ and functional groups in g-C$_3$N$_4$ with a concomitant increase in O—O bond length (see Figure S8 and Table S5 in the supplementary information) indicates that O—O bond becomes weaker, which may lead to breakage of this bond to form OH groups.

Our results indicate that the oxygen is in the structure of g-C$_3$N$_4$ as C=O, C-OH, and N—O functional groups. It is widely reported, mainly in the discussion of the surface chemistry of carbon materials, the redox behavior of oxygenated functional groups, such as hydroquinone/quinone (Eq. (1)) [57].

$$\left(-OH_{surf}\right) \rightleftharpoons H^+ + \left(= O_{surf}\right) + e^- \tag{1}$$

$$H_2O_2 + e^- + H^+ \rightarrow H_2O + OH^· \tag{2}$$

Recently, Navalon et al. have investigated the effect of hydroquinone/quinone-like functional groups present in reduced graphene oxide (rGO) and have suggested, following DFT calculations and the use of simple molecules of organocatalysts, that these functional groups could activate the formation of HO$^•$ radicals (Eq. (2)) by H$_2$O$_2$ in a similar way to the homogeneous metal-promoted Fenton reaction [58]. In addition, the preparation of g-C$_3$N$_4$ in an oxidizing atmosphere enables the oxidation of amines leading to the formation of hydroxylamine-like structures, –NH-OH, which may act as reducing agents according to Eq. (3).

$$\left(-NHOH_{surf}\right) \rightarrow 2H^+ + -NO + 2e^- \tag{3}$$
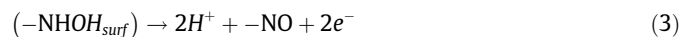
We used the DMPO test to provide evidence of the formation of hydroxyl radicals from our as-synthesized samples of g-C$_3$N$_4$ in the presence of H$_2$O$_2$. Fig. 10 shows the DMPO spin-trapping EPR
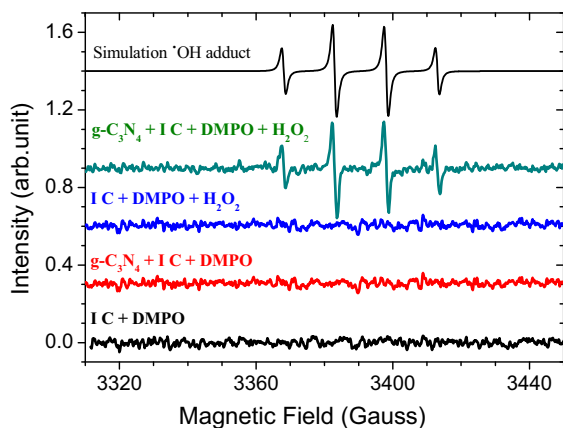
Fig. 10. Room temperature EPR spectra of DMPO_HO$^\bullet$ radical adduct and the controls of the reaction of CNO-600 with IC and H_2O_2 as well as the spectral simulation of the DMPO_HO$^\bullet$ adduct.

spectra for the representative g-C$_3$N$_4$ sample obtained at 600 °C (g-C$_3$N$_4$ + IC + DMPO + H$_2$O$_2$) and some control samples (IC + DMPO, g-C$_3$N$_4$ + IC + DMPO and IC + DMPO + H$_2$O$_2$), besides the simulation for the DMPO_HO radical adduct spectra [41]. It is clear that the four characteristic peaks of DMPO_HO$^\bullet$ adduct with intensity ratio of 1:2:2:1 were observed only in the presence of both g-C$_3$N$_4$ and H$_2$O$_2$.

Additionally, another measurement was performed to analyze the DMPO_HO$^\bullet$ adduct signal for the mixture g-C$_3$N$_4$ + IC + DMPO + H$_2$O$_2$ inside the EPR cell, before and after 70 min. As can be seen in Fig. 11, the signal of the DMPO_HO adduct was increased by 29%, which indicates the formation of oxidizing radicals. These results supply a proof of the metal-free heterogeneous Fenton-like reaction of g-C$_3$N$_4$ in the presence of H$_2$O$_2$ probably by action of the HO$^\bullet$ radicals to degrade IC even under dark conditions.

In fact, some unexplored studies with EPR have shown the ability of g-C$_3$N$_4$ to form hydroxyl radicals in the presence of H$_2$O$_2$ [21]. Thus, a similar behavior can be anticipated with g-C$_3$N$_4$, that is, the formation of hydroxyl radicals through the reduction and/or oxidation of 1 electron of H$_2$O$_2$ in reactions similar to those observed in the traditional homogeneous Fenton reaction, with Fe^{2+} and Fe^{3+}.

In the traditional Fenton reaction, pH is a very important variable. It is known that at very acidic pH, the Fenton reaction is impaired due to the elimination of radicals by the H$^+$ ions and/or
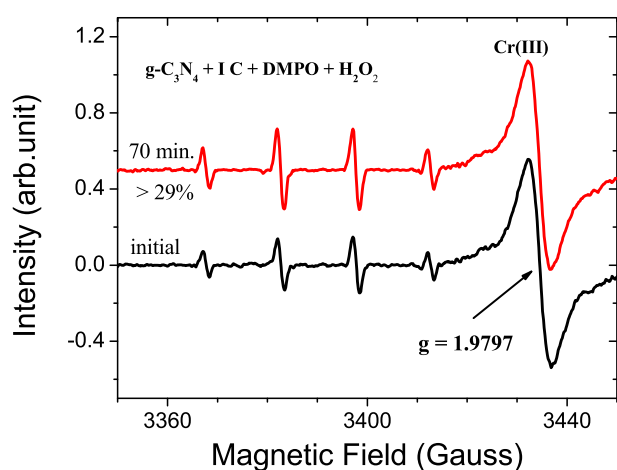

Fig. 12. pH influence on the catalytic activity of heterogeneous Fenton-Like reaction using the g-C$_3$N$_4$ sample prepared at 500 °C. Conditions: [IC] = 20 mg L^{-1} and [H$_2$O$_2$] = 3.9 × 10^{-3} mol L^{-1}.

oxonium ion [H$_3$O$_2$]$^+$ formation. In addition, in acidic medium, the traditional heterogeneous Fenton based on some metallic compounds cannot be used, for example, some iron (III) oxides and hydroxides. Since the H$^+$ ions participate in the equilibrium, in the Fenton-like reaction proposed here, we monitor the pH during the discoloration of the dye IC (Figure S9). As can be clearly seen, the pH of the system decreases during the reaction, suggesting a reaction mechanism with the release of H$^+$ ions. In this way, we conducted the dye discoloration reaction at pH 3 and 6. As shown in Fig. 12, lowering the pH leads to a small decrease in the dye discoloration rate. Under less acidic conditions, the chemical equilibrium presented in equations (1) and (3) are favored, the concentration of protonated H$_2$O$_2$ species is very low and the decrease in oxidation potential is relatively small.

In order to investigate the presence of NH-OH and C-OH functional groups, which can potentially form hydroxyl radicals by reducing H$_2$O$_2$, we conducted a subsequent oxidative treatment of the g-C$_3$N$_4$ sample (prepared at 500 °C) with 5 M H$_2$O$_2$ at 80 °C for 2 h. After reaction with H$_2$O$_2$, the sample was re-tested for IC discoloration. The obtained result (Fig. 13) shows the

Fig. 11. EPR spectra of DMPO_HO$^\bullet$ radical adduct inside the EPR cell in the initial time and after 70 min. The signal of the Cr(III) as impurity in MgO crystal was used as reference for the intensity and calibration of the magnetic field.
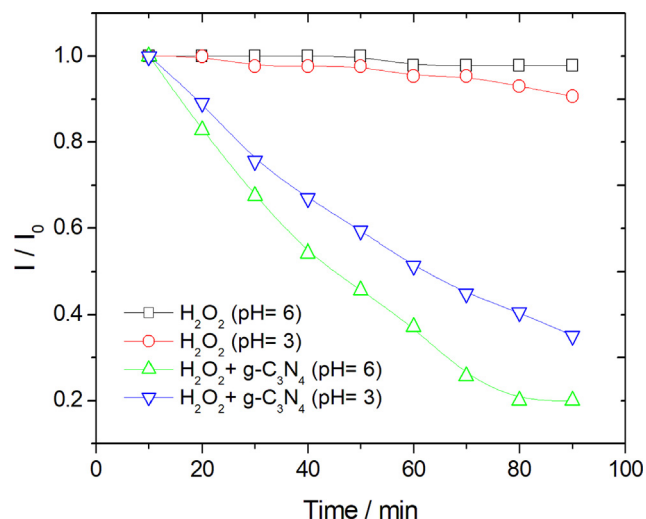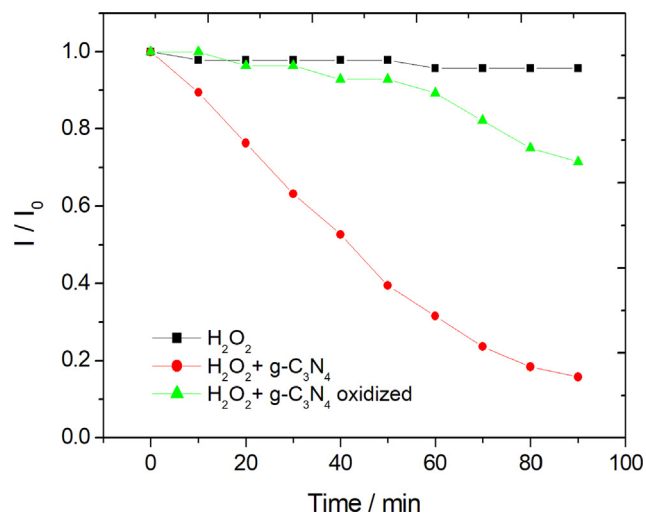

Fig. 13. Effect of H$_2$O$_2$ treatment on the catalytic activity of g-C$_3$N$_4$ sample prepared at 500 °C. Conditions: pH = 6, [IC] = 20 mg L^{-1} and [H$_2$O$_2$] = 3.9 × 10^{-3} mol L^{-1}.

decrease in the dye discoloration rate, indicating that previous treatment of g-C_3N_4 with H_2O_2 eliminates some functional groups that contribute to the formation of oxidizing radicals.

4. Conclusions

Graphitic carbon nitrides were obtained from the polycondensation of melamine after heat treatments under air atmosphere between 500 and 600 °C. These catalysts proved to be efficient to degrade indigo carmine with H_2O_2 through the formation of HO$^\bullet$ radicals in the absence of light. We noted that the Fenton-like catalytic activity is directly related to the oxygenated functional groups on the metal-free g-C_3N_4 structure, but without a direct relationship with the specific surface area of the materials. However, the set of results obtained by different characterization techniques (such as XPS, FTIR and solid-state NMR spectroscopy) indicate that during the thermal condensation of melamine at the temperatures studied, reduced oxygenated functional groups such as C-OH and –NH-OH are formed. These groups, in the presence of H_2O_2, can produce oxidizing radicals, which further degrade the indigo carmine dye. The effect of pH as well as the release of H$^+$ ions during discoloration gradation suggests, together with the results of EPR, a mechanism involving hydroxyl radicals. The oxygenated g-C_3N_4 has been shown to be a promising metal-free catalysts for Fenton-like oxidation reactions. In addition, the new information on g-C_3N_4 surface reactivity may contribute to future research on the use of g-C_3N_4 as a catalyst and chemical platform for different functionalization reactions. Finally, the presence of reducing sites on the surface of g-C_3N_4 can be useful in different catalytic processes, for example, CO_2 reduction.

CRediT authorship contribution statement

Wanessa L. Oliveira: Investigation, Methodology, Visualization, Writing - original draft. **Meiriele Antunes Ferreira:** Investigation, Methodology, Visualization, Writing - original draft. **Henrique A. J.L. Mourão:** Writing - original draft, Supervision. **Manoel J.M. Pires:** Writing - original draft, Writing - review & editing. **Vinícius Ferreira:** Investigation. **Honória F. Gorgulho:** Investigation, Resources. **Daniel F. Cipriano:** Resources, Investigation, Writing - original draft. **Jair C.C. Freitas:** Resources, Investigation, Writing - original draft. **Valmor R. Mastelaro:** Resources, Writing - review & editing. **Otaciro R. Nascimento:** Resources, Writing - review & editing. **Dalva E.C. Ferreira:** Investigation, Writing - original draft. **Frederico Ramos Fioravante:** Investigation, Writing - review & editing. **Márcio C. Pereira:** Writing - review & editing. **João P. de Mesquita:** Supervision, Writing - original draft.

Declaration of Competing Interest

The authors declare that they have no known competing financial interests or personal relationships that could have appeared to influence the work reported in this paper.

Appendix A. Supplementary material

Supplementary data to this article can be found online at https://doi.org/10.1016/j.jcis.2020.12.031.

References

[1] D.R. Dreyer, C.W. Bielawski, Carbocatalysis: heterogeneous carbons finding utility in synthetic chemistry, Chem. Sci. 2 (7) (2011) 1233–1240.

[2] Z.X. Pei, J.X. Zhao, Y. Huang, M.S. Zhu, Z.F. Wang, Z.F. Chen, C.Y. Zhi, Toward enhanced activity of a graphitic carbon nitride-based electrocatalyst in oxygen reduction and hydrogen evolution reactions via atomic sulfur doping, J. Mater. Chem. A 4 (31) (2016) 12205–12211.

[3] A.W. Wang, C.D. Wang, L. Fu, W.N. Wong-Ng, Y.C. Lan, Recent advances of graphitic carbon nitride-based structures and applications in catalyst, sensing, imaging, and LEDs, Nano-Micro Letters 9 (4) (2017).

[4] L. Zhou, H.Y. Zhang, H.Q. Sun, S.M. Liu, M.O. Tade, S.B. Wang, W.Q. Jin, Recent advances in non-metal modification of graphitic carbon nitride for photocatalysis: a historic review, Catal. Sci. Technol. 6 (19) (2016) 7002–7023.

[5] L. Qu, Y. Liu, J.-B. Baek, L. Dai, Nitrogen-doped graphene as efficient metal-free electrocatalyst for oxygen reduction in fuel cells, ACS Nano 4 (3) (2010) 1321–1326.

[6] J.L. Figueiredo, Functionalization of porous carbons for catalytic applications, J. Mater. Chem. A 1 (33) (2013) 9351–9364.

[7] A.D. Bokare, W. Choi, Review of iron-free Fenton-like systems for activating H2O2 in advanced oxidation processes, J. Hazard. Mater. 275 (2014) 121–135.

[8] E.G. Garrido-Ramírez, B.K.G. Theng, M.L. Mora, Clays and oxide minerals as catalysts and nanocatalysts in Fenton-like reactions — a review, Appl. Clay Sci. 47 (3) (2010) 182–192.

[9] J.C. Espinosa, S. Navalón, A. Primo, M. Moral, J.F. Sanz, M. Álvaro, H. García, Graphenes as efficient metal-free Fenton catalysts, Chem. – Eur. J. 21 (34) (2015) 11966–11971.

[10] Y. Zhao, W.-F. Chen, C.-F. Yuan, Z.-Y. Zhu, L.-F. Yan, Hydrogenated graphene as metal-free catalyst for Fenton-like reaction, Chin. J. Chem. Phys. 25 (3) (2012) 335–338.

[11] L. Lyu, G. Yu, L. Zhang, C. Hu, Y. Sun, 4-Phenoxyphenol-functionalized reduced graphene oxide nanosheets: a metal-free Fenton-like catalyst for pollutant destruction, Environ. Sci. Technol. 52 (2) (2018) 747–756.

[12] J.C. Espinosa, S. Navalón, M. Álvaro, H. García, Reduced graphene oxide as a metal-free catalyst for the light-assisted Fenton-like reaction, ChemCatChem 8 (16) (2016) 2642–2648.

[13] X. Wang, K. Maeda, A. Thomas, K. Takanabe, G. Xin, J.M. Carlsson, K. Domen, M. Antonietti, A metal-free polymeric photocatalyst for hydrogen production from water under visible light, Nat. Mater. 8 (2008) 76.

[14] J. Wen, J. Xie, X. Chen, X. Li, A review on g-C3N4-based photocatalysts, Appl. Surf. Sci. 391 (2017) 72–123.

[15] J.J. Zhu, P. Xiao, H.L. Li, S.A.C. Carabineiro, Graphitic carbon nitride: synthesis, properties, and applications in catalysis, ACS Appl. Mater. Interfaces 6 (19) (2014) 16449–16465.

[16] X. Li, Y. Pi, L. Wu, Q. Xia, J. Wu, Z. Li, J. Xiao, Facilitation of the visible light-induced Fenton-like excitation of H2O2 via heterojunction of g-C3N4/NH2-Iron terephthalate metal-organic framework for MB degradation, Appl. Catal. B 202 (2017) 653–663.

[17] J. Ma, Q. Yang, Y. Wen, W. Liu, Fe-g-C3N4/graphitized mesoporous carbon composite as an effective Fenton-like catalyst in a wide pH range, Appl. Catal. B 201 (2017) 232–240.

[18] L. Zhou, L. Wang, J. Zhang, J. Lei, Y. Liu, Well-dispersed Fe2O3 nanoparticles on g-C3N4 for efficient and stable photo-Fenton photocatalysis under visible-light irradiation, Eur. J. Inorg. Chem. 2016 (34) (2016) 5387–5392.

[19] J. Xiao, Y. Xie, H. Cao, Y. Wang, Z. Zhao, g-C3N4-triggered super synergy between photocatalysis and ozonation attributed to promoted OH generation, Catal. Commun. 66 (2015) 10–14.

[20] S.C. Yan, Z.S. Li, Z.G. Zou, Photodegradation performance of g-C3N4 fabricated by directly heating melamine, Langmuir 25 (17) (2009) 10397–10401.

[21] Y. Cui, Z. Ding, P. Liu, M. Antonietti, X. Fu, X. Wang, Metal-free activation of H2O2 by g-C3N4 under visible light irradiation for the degradation of organic pollutants, PCCP 14 (4) (2012) 1455–1462.

[22] L. Jiang, X. Yuan, G. Zeng, X. Chen, Z. Wu, J. Liang, J. Zhang, H. Wang, H. Wang, Phosphorus- and sulfur-codoped g-C3N4: facile preparation, mechanism insight, and application as efficient photocatalyst for tetracycline and methyl orange degradation under visible light irradiation, ACS Sust. Chem. Eng. 5 (7) (2017) 5831–5841.

[23] Q. Xiang, J. Yu, M. Jaroniec, Preparation and enhanced visible-light photocatalytic H2-production activity of graphene/C3N4 composites, J. Phys. Chem. C 115 (15) (2011) 7355–7363.

[24] C. Song, M. Fan, W. Shi, W. Wang, High-performance for hydrogen evolution and pollutant degradation of reduced graphene oxide/two-phase g-C3N4 heterojunction photocatalysts, Environ. Sci. Pollut. Res. 25 (15) (2018) 14486–14498.

[25] Y. Tao, Q. Ni, M. Wei, D. Xia, X. Li, A. Xu, Metal-free activation of peroxymonosulfate by g-C3N4 under visible light irradiation for the degradation of organic dyes, RSC Adv. 5 (55) (2015) 44128–44136.

[26] N. Sun, Y. Liang, X. Ma, F. Chen, Reduced oxygenated g-C3N4 with abundant nitrogen vacancies for visible-light photocatalytic applications, Chem. – Eur. J. 23 (61) (2017) 15466–15473.

[27] G.N. Li, L. Li, H.Y. Yuan, H.F. Wang, H.R. Zeng, J.L. Shi, Alkali-assisted mild aqueous exfoliation for single-layered and structure-preserved graphitic carbon nitride nanosheets, J. Colloid Interface Sci. 495 (2017) 19–26.

[28] N. Jiang, L. Lyu, G. Yu, L. Zhang, C. Hu, A dual-reaction-center Fenton-like process on –C□N–Cu linkage between copper oxides and defect-containing g-

C3N4 for efficient removal of organic pollutants, J. Mater. Chem. A 6 (36) (2018) 17819–17828.

[29] H.J. Yu, R. Shi, Y.X. Zhao, T. Bian, Y.F. Zhao, C. Zhou, G.I.N. Waterhouse, L.Z. Wu, C.H. Tung, T.R. Zhang, Alkali-assisted synthesis of nitrogen deficient graphitic carbon nitride with tunable band structures for efficient visible-light-driven hydrogen evolution, Adv. Mater. 29 (16) (2017).

[30] F. Wei, Y. Liu, H. Zhao, X. Ren, J. Liu, T. Hasan, L. Chen, Y. Li, B.-L. Su, Oxygen self-doped g-C3N4 with tunable electronic band structure for unprecedentedly enhanced photocatalytic performance, Nanoscale 10 (9) (2018) 4515–4522.

[31] H.A. Bicalho, J.L. Lopez, I. Binatti, P.F.R. Batista, J.D. Ardisson, R.R. Resende, E. Lorençon, Facile synthesis of highly dispersed Fe(II)-doped g-C3N4 and its application in Fenton-like catalysis, Mol. Catal. 435 (2017) 156–165.

[32] B.R.S. Lemos, I.F. Teixeira, B.F. Machado, M.R.A. Alves, J.P. de Mesquita, R.R. Ribeiro, R.R. Bacsa, P. Serp, R.M. Lago, Oxidized few layer graphene and graphite as metal-free catalysts for aqueous sulfide oxidation, J. Mater. Chem. A 1 (33) (2013) 9491–9497.

[33] D.R.d.S. Souza, J.P.d. Mesquita, R.M. Lago, L.D. Caminhas, F.V. Pereira, Cellulose nanocrystals: a versatile precursor for the preparation of different carbon structures and luminescent carbon dots, Ind. Crops Prod. 93 (2016) 121–128.

[34] L.A. Alves, A.H. de Castro, F.G. de Mendonça, J.P. de Mesquita, Characterization of acid functional groups of carbon dots by nonlinear regression data fitting of potentiometric titration curves, Appl. Surf. Sci. 370 (2016) 486–495.

[35] D. Briggs, Handbook of X-ray Photoelectron Spectroscopy C. D. Wanger, W. M. Riggs, L. E. Davis, J. F. Moulder and G. E.Muilenberg Perkin-Elmer Corp., Physical Electronics Division, Eden Prairie, Minnesota, USA, 1979. 190 pp. $195, Surface and Interface Analysis 3(4) (1981) v–v.

[36] K.L. Tan, B.T.G. Tan, E.T. Kang, K.G. Neoh, X-ray photoelectron spectroscopy studies of the chemical structure of polyaniline, Phys. Rev. B 39 (11) (1989) 8070–8073.

[37] X. Zhou, H. Li, J. Yang, Biomass-derived activated carbon materials with plentiful heteroatoms for high-performance electrochemical capacitor electrodes, J. Energy Chem. 25 (1) (2016) 35–40.

[38] A. Thomas, A. Fischer, F. Goettmann, M. Antonietti, J.O. Muller, R. Schlogl, J.M. Carlsson, Graphitic carbon nitride materials: variation of structure and morphology and their use as metal-free catalysts, J. Mater. Chem. 18 (41) (2008) 4893–4908.

[39] T.C. Araújo, H.d.S. Oliveira, J.J.S. Teles, J.D. Fabris, L.C.A. Oliveira, J.P. de Mesquita, Hybrid heterostructures based on hematite and highly hydrophilic carbon dots with photocatalytic activity, Appl. Catal. B 182 (2016) 204–212.

[40] H.R. Rajabi, O. Khani, M. Shamsipur, V. Vatanpour, High-performance pure and Fe3+-ion doped ZnS quantum dots as green nanophotocatalysts for the removal of malachite green under UV-light irradiation, J. Hazard. Mater. 250–251 (2013) 370–378.

[41] S. Stoll, A. Schweiger, EasySpin, a comprehensive software package for spectral simulation and analysis in EPR, J. Magn. Reson. 178 (1) (2006) 42–55.

[42] M.J. Bojdys, J.O. Muller, M. Antonietti, A. Thomas, Ionothermal synthesis of crystalline, condensed, graphitic carbon nitride, Chem. – Eur. J. 14 (27) (2008) 8177–8182.

[43] B. Jurgens, E. Irran, J. Senker, P. Kroll, H. Muller, W. Schnick, Melem (2,5,8-triamino-tri-s-triazine), an important intermediate during condensation of melamine rings to graphitic carbon nitride: synthesis, structure determination by X-ray powder diffractometry, solid-state NMR, and theoretical studies, J. Am. Chem. Soc. 125 (34) (2003) 10288–10300.

[44] Pavia D.L., Lampman G.M., Kriz G.S., Vyvyan J.R., Introdução a Espectroscopia, second ed., Cengage Learning, São Paulo, Brasil, 2015.

[45] H.-J. Li, B.-W. Sun, B. Sui, D.-J. Qian, M. Chen, Preparation of water-dispersible porous g-C3N4 with improved photocatalytic activity by chemical oxidation, PCCP 17 (5) (2015) 3309–3315.

[46] F. Dong, Y. Li, Z. Wang, W.-K. Ho, Enhanced visible light photocatalytic activity and oxidation ability of porous graphene-like g-C3N4 nanosheets via thermal exfoliation, Appl. Surf. Sci. 358 (2015) 393–403.

[47] B. Zhu, P. Xia, W. Ho, J. Yu, Isoelectric point and adsorption activity of porous g-C3N4, Appl. Surf. Sci. 344 (2015) 188–195.

[48] Y. Hu, Y. Shim, J. Oh, S. Park, S. Park, Y. Ishii, Synthesis of 13C-,15N-labeled graphitic carbon nitrides and NMR-based evidence of hydrogen-bonding assisted two-dimensional assembly, Chem. Mater. 29 (12) (2017) 5080–5089.

[49] Y. Li, H. Xu, S. Ouyang, D. Lu, X. Wang, D. Wang, J. Ye, In situ surface alkalinized g-C3N4 toward enhancement of photocatalytic H2 evolution under visible-light irradiation, J. Mater. Chem. A 4 (8) (2016) 2943–2950.

[50] L. Yang, J. Huang, L. Shi, L. Cao, Q. Yu, Y. Jie, J. Fei, H. Ouyang, J. Ye, A surface modification resultant thermally oxidized porous g-C3N4 with enhanced photocatalytic hydrogen production, Appl. Catal. B 204 (2017) 335–345.

[51] Y.-H. Lee, Y.-F. Lee, K.-H. Chang, C.-C. Hu, Synthesis of N-doped carbon nanosheets from collagen for electrochemical energy storage/conversion systems, Electrochem. Commun. 13 (1) (2011) 50–53.

[52] H. Guo, Y. Ren, Q. Cheng, D. Wang, Y. Liu, Gold nanoparticles on cyanuric acid-based support: a highly active catalyst for the reduction of 4-nitrophenol in water, Catal. Commun. 102 (2017) 136–140.

[53] A.P. Dementjev, A. de Graaf, M.C.M. van de Sanden, K.I. Maslakov, A.V. Naumkin, A.A. Serov, X-ray photoelectron spectroscopy reference data for identification of the C3N4 phase in carbon–nitrogen films, Diam. Relat. Mater. 9 (11) (2000) 1904–1907.

[54] J. Li, B. Shen, Z. Hong, B. Lin, B. Gao, Y. Chen, A facile approach to synthesize novel oxygen-doped g-C3N4 with superior visible-light photoreactivity, Chem. Commun. 48 (98) (2012) 12017–12019.

[55] J. Hu, J. Wang, T.H. Nguyen, N. Zheng, The chemistry of amine radical cations produced by visible light photoredox catalysis, Beilstein J. Org. Chem. 9 (2013) 1977–2001.

[56] P. Wu, P. Du, H. Zhang, C. Cai, Microscopic effects of the bonding configuration of nitrogen-doped graphene on its reactivity toward hydrogen peroxide reduction reaction, PCCP 15 (18) (2013) 6920–6928.

[57] K. Kinoshita, Carbon: electrochemical and physicochemical properties, first ed., Wiley Interscience, 1988.

[58] S. Navalon, A. Dhakshinamoorthy, M. Alvaro, M. Antonietti, H. García, Active sites on graphene-based materials as metal-free catalysts, Chem. Soc. Rev. 46 (15) (2017) 4501–4529.